The flux tube and the flux tube breaking amplitude in the harmonic approximation

1987 J. Phys. G: Nucl. Phys. 13 423

(http://iopscience.iop.org/0305-4616/13/4/005)

J. Phys. G: Nucl. Phys. **13** (1987) 423–438. Printed in the UK

The flux tube and the flux tube breaking amplitude in the harmonic approximation

Nigel Dowrick†, Jack Paton and Stavros Perantonis‡
Department of Theoretical Physics, 1 Keble Road, Oxford, UK

Received 16 May 1986

Abstract. In the flux tube model the amplitude for meson hadronic decay $A \to B + C$ is given by an overlap integral containing a factor γ^a_{bc} which represents the amplitude that the initial flux tube a should break at a specific point, forming the two flux tubes b and c of the final two mesons. We estimate the factor γ^a_{bc} in a harmonic approximation for the decays of both ordinary quark model mesons (a = flux tube ground state) and the lowest vibrational hybrids (a = first excited state of flux tube). We also discuss the relationship of the flux tube model to the leading term in the evaluation of the Wilson loop expectation value.

1. Introduction

In the flux tube model [1], which is abstracted from the lattice Hamiltonian version of QCD introduced by Kogut and Susskind [2], hadrons are regarded on the scale $a \sim 0.1$–0.2 fm for which the coupling $g(a) \sim 1$ as quarks connected by lines of chromoelectric flux or flux tubes. The flux may exist in one of several topologies. In the lowest lying mesons the flux tube topology is just that of a single string joining a quark–antiquark pair. The flux tube carries mass per unit length $b \sim 1$ GeV fm^{-1} and is a quantum object with (in the adiabatic limit of fixed quark and antiquark positions) a spectrum of states. Each quantum state of the flux tube defines an adiabatic potential surface for quark motion. The mesons of the usual quark model are identified with the adiabatic surface in which the flux tube is in its ground state, and other surfaces correspond to so-called 'vibrational hybrid' states which are additional to the states of the naive quark model.

The flux tube model leads naturally to a mechanism for hadron decay which is very similar to that of the $^3P_0$ quark pair creation (QPC) model [3]. The difference is that in the flux tube model the $q\bar{q}$ pair is created with an amplitude which is proportional to the overlap between the initial and final flux tube wavefunctions [4]. Specifically for the decay of a meson A to mesons B and C with quark relative wavefunctions ψ_A, ψ_B, ψ_C the amplitude is proportional to

$$M(A \to BC) = \int d^3\boldsymbol{r} \int d^3\boldsymbol{w}\, \psi^*_B(\tfrac{1}{2}\boldsymbol{r} + \boldsymbol{w})\psi^*_C(\tfrac{1}{2}\boldsymbol{r} - \boldsymbol{w})\alpha \cdot (i\nabla_B + i\nabla_C + \boldsymbol{q})\psi_A(\boldsymbol{r}) \exp(\tfrac{1}{2}i\boldsymbol{q}\cdot\boldsymbol{r})\gamma^a_{bc}(\boldsymbol{r}, \boldsymbol{w})$$

where the limit $\gamma^a_{bc} =$ constant corresponds to the QPC model, $\boldsymbol{q}$ is the CM momentum of mesons B and C, and the flux tube breaks at the point of position vector $\boldsymbol{w}$. The initial

† Vacation project student, supported in part by Merton College, Oxford.
‡ Supported in part by the Alexander S Onassis Public Benefit Foundation.

0305-4616/87/040423 + 16 $02.50

quark–antiquark pair are at $\pm \boldsymbol{r}/2$. It has been pointed out [4] that decays between quark model mesons ($a=b=c=0$) are not very sensitive to the functional form of γ^0_{00} and thus the successes of the QPC decay model are reproduced. Nevertheless the relation between γ^1_{00} and γ^0_{00} allows a parameter-free calculation of the decay amplitude of hybrid mesons [5].

We present in the next section the results of a calculation of γ^a_{bc} in a harmonic approximation to the flux tube motion. Although a more realistic calculation is possible [6] it is considerably more complicated, and the simple picture presented here should have some qualitative validity.

2. The harmonic approximation

The flux tube joining a quark–antiquark pair a distance $r=(N+1)a$ apart is modelled as a set of point masses $m=ba$ ($b=$ string tension $\simeq 1$ GeV fm^{-1}) a distance a apart with Lagrangian ($c=\hbar=1$)

$$L=\tfrac{1}{2}m\sum \boldsymbol{y}_i^2-(b/2a)\sum_i (\boldsymbol{y}_{i+1}-\boldsymbol{y}_i)^2 \tag{1}$$

where the $\boldsymbol{y}$s are the transverse displacements of the point masses. The system decouples in terms of (transverse) normal mode coordinates

$$\boldsymbol{a}_i=\sum_{j=1}^{N}\left(\frac{2}{N+1}\right)^{1/2}\boldsymbol{y}_j \sin\left(\frac{ij\pi}{N+1}\right) \tag{2}$$

giving normal frequencies $w_i=(2/a)\sin[i\pi/2(N+1)]$, $i=1, 2, \ldots, N$. The ground state wavefunction is

$$\Psi_0(\{\boldsymbol{y}_i\})=\prod_{i=1}^{N}\frac{\alpha_i}{\pi^{1/2}}\exp(-\tfrac{1}{2}\alpha_i^2\boldsymbol{a}_i^2) \qquad \alpha_i=(w_i m)^{1/2} \tag{3a}$$

and the excited states are of the form ($\Psi_0 \times$ polynomial in $\boldsymbol{a}_i$). For example, the wavefunctions of the first excited states are

$$\Psi_1^{\pm}(\{\boldsymbol{y}_i(x)\})=\alpha_1(a_1^x \pm \mathrm{i}a_1^y)\Psi_0(\{\boldsymbol{y}_i(x)\}). \tag{3b}$$

In any state j we can define a flux density function

$$\rho_j(N, N_b, \boldsymbol{y}_b)=\prod_{i=1}^{N}\int \mathrm{d}^2 y_i' |\Psi_j(\{\boldsymbol{y}_i'\})|^2 \delta(\boldsymbol{y}_b-\boldsymbol{y}_b'). \tag{4}$$

In particular for the flux tube ground state, ρ_0 has a gaussian dependence on $\boldsymbol{y}_b$ with a 'diameter' between half maximum points which depends somewhat on quark–antiquark separation $r=Na$ and on distance along the quark–antiquark axis $\xi r=N_b a$ ($0\leqslant\xi\leqslant 1$). A numerical calculation of this is shown in figures 1 and 2. Thus the flux tube is rather fat, because of quantum fluctuations, and its diameter increases logarithmically with its length asymptotically.

We now obtain expressions for the amplitude γ^a_{bc} for the initial flux tube with wavefunction Ψ_a to break at the point $(N_b, \boldsymbol{y}_b)$ into two flux tubes with wavefunctions Ψ_{bL} and Ψ_{cR} (see appendix to reference [4]). The axes of the final flux tubes do not coincide with that of the initial flux tube, so it is necessary to introduce new coordinates $\boldsymbol{y}_i^L$, $\boldsymbol{y}_i^R$ to

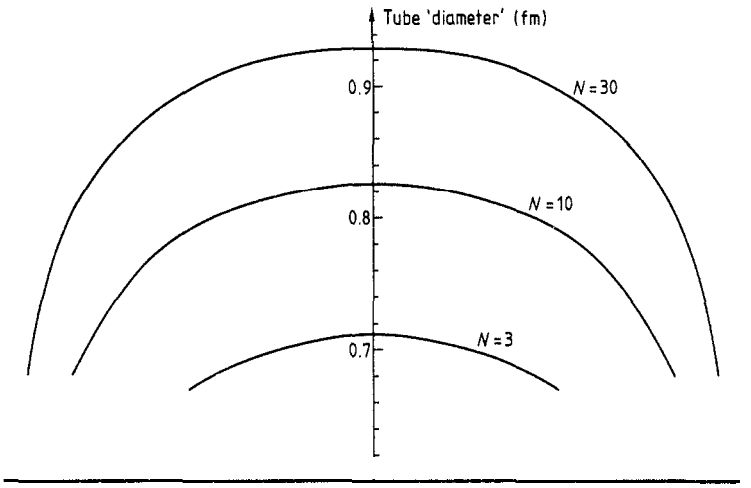

Figure 1. Flux tube 'diameter' at different places along the string for different values of N. N is related to the quark–antiquark separation r by $r=Na$ (a such that $g(a)\sim 1$ is $a=0.1$–0.2 fm). The 'diameter' is measured in fm, taking the string tension $b=1$ GeV fm^{-1}.

describe their configurations. To first order

$$y_i^{\mathrm{L}} = y_i - \frac{i}{N_{\mathrm{b}}} y_{\mathrm{b}} \qquad y_i^{\mathrm{R}} = y_i - \frac{N+1-i}{N+1-N_{\mathrm{b}}} y_{\mathrm{b}}$$

and if all the flux tubes are in their ground states we have

$$\gamma_{00}^{0} = \prod_i \int \mathrm{d}^2 y_i' K \exp(-C_{ij} y_i' \cdot y_j') \delta(y_{\mathrm{b}}' - y_{\mathrm{b}}) \tag{5}$$

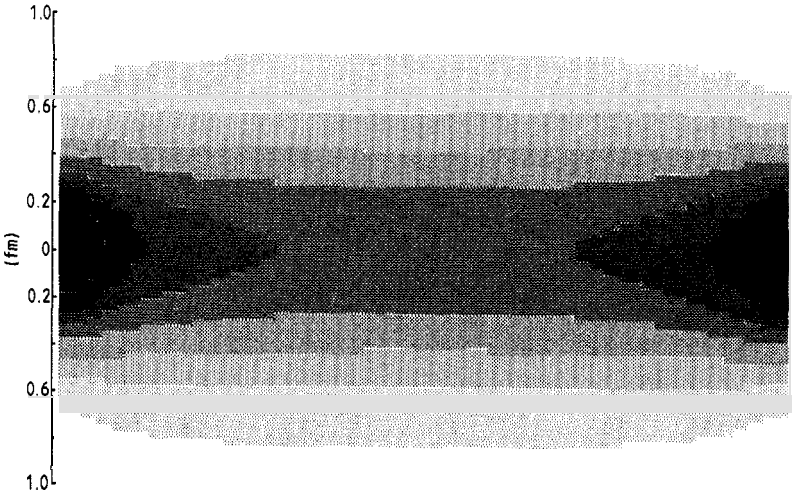

Figure 2. Flux density function ρ_0 for the flux tube ground state. The quark and antiquark are situated at the extremes of the horizontal axis a distance $31a$ apart. The transverse scale assumes the string tension $b=1$ GeV fm^{-1}. The longitudinal and transverse scales are identical for $a=0.1$ fm.

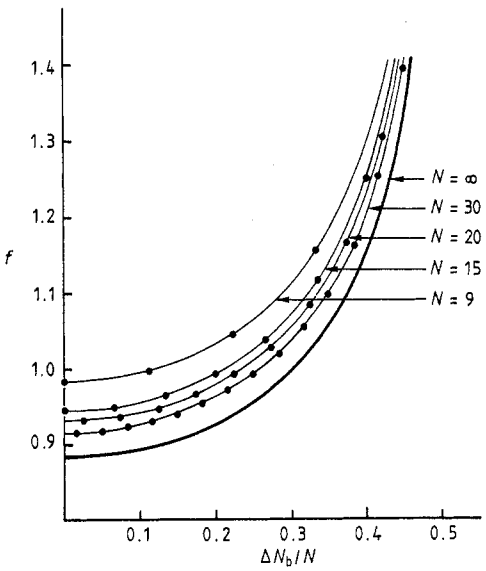

Figure 3. The string breaking amplitude γ^{a}_{bc} has the form (polynomial in y_b $\exp(-\frac{1}{2}fby_b^2)$. This is a plot of the gaussian coefficient f as a function of relative position along the flux tube for various values of $N(\Delta Nb = |\frac{1}{2}(N+1) - N_b|)$. The curve labelled $N = \infty$ corresponds to the continuum limit f_c of f.

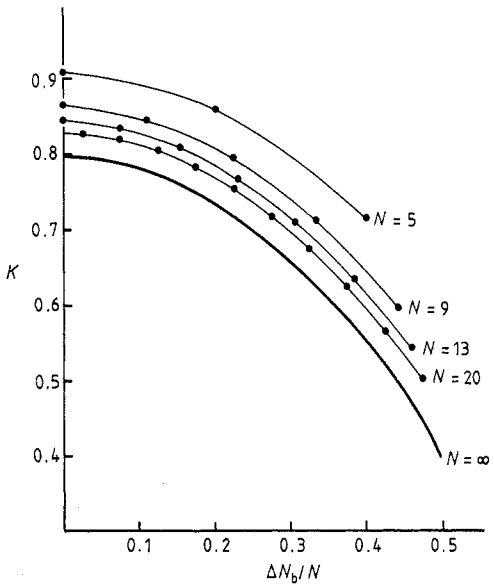

Figure 4. The ratio of the string breaking amplitude for flux tube excited and ground state $\gamma^1_{00}/\gamma^0_{00}$ has the form $\gamma^1_{00}/\gamma^0_{00} = \kappa\sqrt{b}y_{b\pm}$. Here is plotted the coefficient κ as a function of relative position along the flux tube for various values of N. The curve labelled $N = \infty$ corresponds to the continuum limit κ_c of κ.

where K and C_{ij} are independent of the y_i and easily determined. The multiple integral may be integrated by standard means giving

$$\gamma^0_{00} = A^0_{00}(N, N_b)\left(\frac{f(N, N_b)b}{\pi}\right)^{1/2} \exp[-\tfrac{1}{2}f(N, N_b)by_b^2] \tag{6}$$

where A^0_{00} and f are obtained numerically.

It is found that A^0_{00} is independent of N_b to better than 1% for $0 < N < 20$, and decreases slowly with N in this range, $A^0_{00} \sim 1\text{–}0.01N$. For $N \geqslant 10$ the decrease of A^0_{00} becomes logarithmic. The coefficient f is shown as a function of N and N_b in figure 3. For the decay of the flux tube in its first excited state we have

$$\gamma^1_{00} = \kappa\sqrt{b}\, y_b^{\pm}\, \gamma^0_{00} \tag{7}$$

where $y_b^{\pm} = y_{1,b} \pm \mathrm{i}y_{2,b}$ and the coefficient κ is shown as a function of N and N_b in figure 4. We remark further in the next section on the limiting behaviour of the coefficient functions f and κ for large N.

These are all the results required for quark model meson decays [4] and for the decay of the lowest vibrational hybrids [5]. We have also computed the amplitude γ^0_{10} which would be required in the calculation of the decay of a quark model meson to a hybrid, and find that it is quite small,

$$\int (\gamma^0_{10})^2\, \mathrm{d}^2y_b \Big/ \int (\gamma^0_{00})^2\, \mathrm{d}^2y_b \simeq 0.1.$$

3. Connection to the Wilson loop expectation value; the continuum limit

It is clear that the harmonic approximation for the flux tube motion is very crude. The zero-point energy per unit length of the harmonic Hamiltonian is $\sim 0.2/a^2$ GeV fm^{-1} giving 20 GeV fm^{-1} for $a = 0.1$ fm. This is a huge renormalisation of the string tension whose physical value is ~ 1 GeV fm^{-1} and implies that the transverse fluctuations are not small. This is also clear from the shape of the flux density function (figures 1 and 2) which, with $a = 0.1$ fm, has a diameter between half maximum points of 0.8 fm for a quark–antiquark separation of 1 fm. Could it be that the scale $b^{-1/2}$ entering into the wavefunctions in the harmonic approximation, and which determines the scale of the results, is very misleading on account of the inadequacies of this harmonic approximation? The following argument, based on the Wilson loop area law, shows that this is not the case.

According to the Wilson loop area criterion in pure gauge theory, the Wilson loop expectation value with Euclidean time

$$\langle 0|\ \mathrm{Tr} \exp\left(-g \oint_C \sum_i \lambda^i A^i \cdot \mathrm{d}\boldsymbol{r}\right) |0\rangle \tag{8}$$

is proportional to $\exp(-bA)$, where b is the renormalised string tension and C is a loop in space–time spanned by the minimum space–time area A. In all cases to be considered, the boundary conditions will be such that the minimum area surface lies in the hyperplane $y_2 = 0$. Let us choose C to be the loop shown in figure 5(*b*), where the curve $y_1 = y(x)$ is such that

$$|y(x)| \ll L \qquad b^{-1/2} \ll L \ll T. \tag{9}$$

The surface of minimum area $y_1 = V(x, T)$ can actually be determined by minimising the expression for the area

$$A = \int\int \mathrm{d}x\, \mathrm{d}t \left[1 + \left(\frac{\partial v}{\partial x}\right)^2 + \left(\frac{\partial v}{\partial t}\right)^2\right]^{1/2}. \tag{10}$$

To establish contact with our previous discrete harmonic approximation, we note that

$$A \simeq LT + \tfrac{1}{2} \int\int \mathrm{d}x\, \mathrm{d}t \left[\left(\frac{\partial v}{\partial x}\right)^2 + \left(\frac{\partial v}{\partial t}\right)^2\right] \tag{11}$$

where the approximation in (10) is justified by the condition (9) on the curve $y(x)$. The requirement that A, as given by (11), be minimum means that V has to be (approximately) harmonic in x and t.

Introducing the Fourier expansion

$$V(x, t) = (2/L)^{1/2} \sum_{n=1}^{\infty} q_n \sin(n\pi x/L) \exp(-n\pi t/L)$$

where

$$q_n = (2/L)^{1/2} \int_0^L \mathrm{d}x\, y(x) \sin(n\pi x/L) \tag{12}$$

and taking into account (11) and the boundary conditions

$$V(0, t) = V(L, t) = V(x, T) = 0$$

$$V(x, 0) = y(x)$$

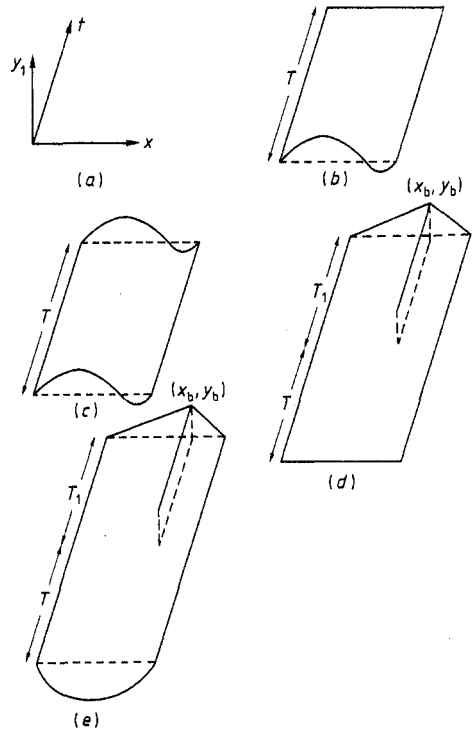

Figure 5. Various bounding loops in space–time. The surfaces are in the hypersurface $y_2 = 0$. (*a*) is the coordinate system used. Each loop contains straight sections $(x=0, y_1=0, t)$ and $(x=0, y_1=L, t)$ between the initial and the final time. Loops (*d*) and (*e*) also contain the straight section $\{(x=x_b, y_1=y_b, t)), t \geqslant 0\}$. The boundaries for the initial and final time and $0 \leqslant x \leqslant L$ are respectively:

(*b*) $(x, y(x), 0); (x, 0, T)$
(*c*) $(x, y(x), -T/2); (x, y(x), T/2)$
(*d*) $(x, 0, -T); (x, y_b x/x_b \theta(x_b - x) + [y_b(1-x)/(L-x_b)]\theta(x-x_b), T_1)$
(*e*) $(x, -h \sin(\pi x/L), -T); (x, y_b x/x_b \theta(x_b - x) + [y_b(1-x)/(L-x_b)]\theta(x-x_b), T_1)$.

we readily find

$$A = LT + \tfrac{1}{2} \sum_n (\pi n/L) q_n^2 . \tag{13}$$

Now the loop expectation value may, for $T \to \infty$, be written as

$$\langle W \rangle = \exp(-E_0 T) \psi_0^*(\{0\}) \psi_0(\{y(x)\}) \tag{14}$$

where E_0 is the ground state energy of the gauge theory in the presence of a source and sink a distance L apart and ψ_0 is the ground state wavefunctional. In the flux tube model the vacuum is just the strong-coupled vacuum and $\psi_0(\{y(x)\})$ is just the wavefunction of the flux tube in its ground state. Noticing that the loop expectation value for the loop defined by the perimeter of an $L \times T$ rectangle is, for $T \to \infty$, given by

$$\exp(-E_0 T) \psi_0^*(\{0\})\, \psi_0(\{0\}) \sim \exp(-bLT) \tag{15}$$

we conclude that

$$\frac{\psi_0(\{y(x)\})}{\psi_0(\{0\})} = \exp\left(-\tfrac{1}{2}b\sum_n \frac{\pi n}{L}\, q_n^2\right). \tag{16}$$

Comparing equations (12) and (16) with equations (2) and (3) we notice that the dependence of ψ_0 on the long-wavelength Fourier components of $y(x)$ is exactly that of our discrete harmonic approximation. We note the correspondence

$$\omega_n \leftrightarrow n\pi/L \qquad m/a \leftrightarrow b. \tag{17}$$

Hence the quantity m/a of the discrete harmonic approximation is replaced by the renormalised string tension b, and thus $b^{-1/2} \sim 0.4$ fm correctly sets the scale of the transverse excursions of the flux tube, as we have assumed. Arguments based on the area law are subject to quantum correction [6], but we see no reason why these should affect the above conclusion. It is to be noted, however, that the harmonic approximation cannot be correct for transverse distances large compared with the $Q\bar{Q}$ separation, since the RHS of (11) is then no longer approximately equal to the area of the surface which spans our space–time loop.

A similar argument based on the area law can be applied to the excited states of the system. Consider the loop in figure 5(*c*) for large (but finite) T. Using the solution $V(x, t)$ of Laplace's equation which obeys the appropriate boundary conditions

$$V(0, t) = V(L, t) = 0$$
$$V(x, T/2) = V(x, -T/2) = y(x)$$

namely

$$V(x, t) = (2/L)^{1/2} \sum_n q_n \operatorname{sech}\left(\frac{n\pi T}{2L}\right) \sin\left(\frac{n\pi x}{L}\right) \cosh\left(\frac{n\pi t}{L}\right)$$

we can calculate the area A by means of equation (11). We find

$$A = LT + \tfrac{1}{2}\sum_n q_n^2 \frac{n\pi}{L} \sinh\left(\frac{n\pi T}{L}\right) \operatorname{sech}^2\left(\frac{n\pi T}{2L}\right). \tag{18}$$

For large T we find

$$A \simeq LT + \sum_n q_n^2 \frac{\pi n}{L}\left[1 - 2\exp(-n\pi T/L)\right]$$

so that for the Wilson loop expectation value we have

$$\langle W\rangle \sim \exp\left[-b\left(LT + \sum_n q_n^2\, \pi n/L\right)\right]\left[1 + 2bq_1^2(\pi/L)\exp(-\pi T/L)\right]. \tag{19}$$

On the other hand, we can write

$$\begin{aligned}\langle W\rangle &= \langle\{y(x)\}|\exp(-HT)|\{y(x)\}\rangle \\ &= \psi_0^*(\{y(x)\})\psi_0(\{y(x)\})\exp(-E_0T) \\ &\quad + \psi_1^*(\{y(x)\})\psi_1(\{y(x)\})\exp(-E_1T) + \ldots\end{aligned} \tag{20}$$

where H is the Hamiltonian of the system, and ψ_0 and ψ_1 denote the wavefunctionals corresponding to the flux tube ground state and to the lowest state of odd symmetry about

the $\bar{Q}Q$ axis and E_0, E_1 are the corresponding values of the energy. Comparing equations (19) and (20) we conclude that

$$E_1 = E_0 + \pi/L \tag{21}$$

$$\frac{\psi_1(\{y(x)\})}{\psi_0(\{y(x)\})} = \left(\frac{2\pi b}{L}\right)^{1/2} q_1 \tag{22}$$

exactly as in the discrete harmonic approximation (cf equation (3*b*)), where π/L is the energy of one quantum of the lowest transverse vibration (cf equation (17)).

Similar arguments can be used to yield information about the string breaking amplitudes γ^{a}_{bc}. Consider, for example, the amplitude γ^{0}_{00}. The amplitude $\langle W_b \rangle$ for the string breaking process depicted in figure 5(*d*) is equal to

$$\langle W_b \rangle = \sum_{I} \langle \{0_L\}, \{0_R\} | \exp(-H_L T_1) \exp(-H_R T_1) | I \rangle \langle I | \exp(-HT) | \{0\} \rangle \tag{23}$$

where the Hamiltonians appearing in the time evolution operators are the ones for the appropriate strings (initial, right or left) and the complete set of intermediate states is subject to the condition that the breaking occurs at the specific point ($x = x_b, y = y_b$). $\langle W_b \rangle$ can be expressed in terms of the overlap integral γ^{0}_{00}

$$\langle W_b \rangle = \psi^{*}_{0,L}(\{0_L\}) \psi^{*}_{0,R}(\{0_R\}) \psi_0(\{0\}) \exp[-E_0 T - (E_{0,L} + E_{0,R}) T_1] \gamma^{0}_{00}. \tag{24a}$$

The energies appearing in the exponent are the ground state energies for the three strings. On the other hand, the area law permits us to write (for large T, T_1)

$$\langle W_b \rangle \propto \exp(-bA) \tag{24b}$$

where A is the area of the minimum area surface which spans the curve in figure 5(*d*). Considering free propagation of the three strings, we find

$$\psi^{*}_{0,L}(\{0_L\}) \psi^{*}_{0,R}(\{0_R\}) \psi_0(\{0\}) \exp[-E_0 T - (E_{0,L} + E_{0,R}) T_1] \propto \exp[-b(A_R + A_L + A_0)] \tag{24c}$$

where A_R, A_L, A_0 are the areas of the rectangles corresponding to the free propagation of the three strings (the initial string is allowed to propagate for time T and the two final strings for T_1). Equations (24) give

$$\gamma^{0}_{00} \propto \exp[-b(A - A_0 - A_R - A_L)]. \tag{25}$$

In order to establish contact with our discrete harmonic approximation, we may use the approximation of equation (11) (which is a good approximation for $|y_b| \ll L$ and for breaking points which are not close to the ends of the initial string). Using this approximation, we can calculate the quantity on the RHS of equation (25). The result is

$$\gamma^{0}_{00} \sim \exp[-b/2 f_c(\rho) y_b^2] \tag{26}$$

where

$$f_c(\rho) = (1/\pi) \ln [(1-\rho)^{-1/\rho} \rho^{-1/1-\rho}] \tag{27}$$

and we have put $\rho = x_b/L$. The details of this calculation are given in appendix 1.

It is evident that the quantity f_c represents the value of the coefficient function f of the harmonic approximation in the continuum limit $N \to \infty$, $N_b \to \infty$, $\rho = N_b/N$ fixed. A plot of f_c against ρ is given in figure 3 along with plots of $f(N, N_b)$ for finite values of N.

Finally, we can use the area law to obtain information about γ_{00}^{1}. Consider the ratio R of the amplitude for the two string breaking processes depicted in figures 5(*d*) and 5(*e*)

$$R=\frac{\Sigma_{\mathrm{I}}\langle\{0_{\mathrm{L}}\},\{0_{\mathrm{R}}\}|\exp(-H_{\mathrm{L}}T_1)\exp(-H_{\mathrm{R}}T_1)|\mathrm{I}\rangle\langle\mathrm{I}|\exp(-HT)|\{-h\sin\pi x/L\}\rangle}{\Sigma_{\mathrm{I}}\langle\{0_{\mathrm{L}}\}\{0_{\mathrm{R}}\}|\exp(-H_{\mathrm{L}}T_1)\exp(-H_{\mathrm{R}}T_1)|\mathrm{I}\rangle\langle\mathrm{I}|\exp(-HT)|\{0\}\rangle} \tag{28}$$

where $q_1=-(L/2)^{1/2}h$ and the complete set of intermediate states $|\mathrm{I}\rangle$ at the time of the breaking is understood to be subject to the condition that the breaking occurs at the specific point $(x=x_{\mathrm{b}}, y=y_{\mathrm{b}})$.

By means of equation (28) we can express R in terms of the overlap integrals γ_{00}^{0} and γ_{00}^{1}

$$R=\frac{\psi_0(\{-h\sin\pi x/L\})}{\psi_0(\{0\})}+\frac{\psi_1(\{-h\sin\pi x/L\})}{\psi_0(\{0\})}\exp[-(E_1-E_0)T]\frac{\gamma_{00}^{1}}{\gamma_{00}^{0}}+\ldots$$

or, by virtue of equation (16), (21) and (22),

$$R=\exp(-\tfrac{1}{4}b\pi h^2)\,[1-h(\pi b)^{1/2}\exp(-\pi T/L)(\gamma_{00}^{1}/\gamma_{00}^{0})+\ldots] \tag{29}$$

On the other hand, the area law gives

$$R=\exp[-b(A_{\mathrm{e}}-A_0)] \tag{30}$$

where A_{e}, A_0 are the areas of the minimum area surfaces spanning the curves in figures 5(*d*) and 5(*e*) for large T and T_1. In appendix 2 we calculate A_{e} in the harmonic approximation. We thus obtain the continuum limit for the ratio $\gamma_{00}^{1}/\gamma_{00}^{0}$ and hence for the quantity $\kappa(N, N_b)$ defined by equation (7). The result is

$$\kappa\xrightarrow{\text{continuum}}\kappa_{\mathrm{c}}(\rho)=(2\pi)^{-1/2}\rho^{-\rho}(1-\rho)^{\rho-1} \tag{31}$$

where, as usual $\rho=x_b/L$. A plot of κ_c against ρ is given in figure 4 along with plots of κ for finite values of N.

We find it interesting that the coefficient functions f and κ have finite continuum limits, although in the spirit of the flux tube model we would expect a finite value of $N\sim 10$ to be more relevant to the physics. On the other hand, we have no independent argument on the limiting behaviour of the quantity A_{00}^{0}. Our numerical results are consistent with A_{00}^{0} decreasing slowly to zero as $N\to\infty$.

Our string breaking amplitude is in the continuum limit very similar to that of the dual string, differing only in the boundary conditions at the ends of the string. In our case we have Dirichlet boundary conditions, whereas for the dual string the boundary conditions are Neumann. We note that it has been shown [8] that the string breaking amplitude of the dual string cannot be defined consistent with the conformal invariance of the string action in other than twenty-six dimensions. Perhaps this is an indication that the continuum limit of A_{00}^{0} should be zero. Happily, the continuum limit is not required in the flux tube model, which is not conformally invariant because of the physical scale a. A quantity which clearly has no continuum limit is the flux density function ρ_0, since, as already remarked, the flux tube 'diameter' has a logarithmic dependence on N and becomes infinite in the continuum limit.

4. Final comments

Figure 2 graphically illustrates the fact that, because of quantum zero-point energy, the

flux tube has a transverse radius of the order of $b^{-1/2} \sim 0.4$ fm. One deficiency of the harmonic approximation is that it does not allow backward excursions of the line of flux from the ends of the flux tube. A more realistic calculation [9] would allow these, thus rounding out the extremities of the flux tube. Taking into account this correction, one finds that for quark–antiquark separations $\lesssim b^{-1/2}$, the flux 'tube' is approximately spherical. This is reminiscent of the bag model [10] although our flux tube does not have a sharp boundary, nor are its properties as a medium necessarily those of the perturbative vacuum, as assumed in the bag model. On the other hand, the vacuum of the flux tube model is just (on scales $\gtrsim a \simeq 0.1$–0.2 fm) the strong coupled vacuum which has $\langle E^2 \rangle_a = 0$ and hence $\langle B^2 \rangle_a \neq 0$ since the components of $\boldsymbol{E}$ and $\boldsymbol{B}$ are conjugate variables. Thus the long-wavelength contributions to $\langle F^2 \rangle_{\text{vac}}$ are magnetic, agreeing with the sign of the condensate obtained from sum rules [11].

Acknowledgment

We thank Nathan Isgur for his collaboration in the initial stage of this work.

Appendix 1

In this appendix we calculate the continuum limit f_c of the quantity $f(N, N_b)$ as given by equation (26). In the region shown in figure 6(*a*) we introduce the complex variable $\omega = x + it$. In order to solve our Dirichlet problem

$$\frac{\partial^2 v}{\partial x^2} + \frac{\partial^2 v}{\partial t^2} = 0$$

$$v(x=0, t) = v(x=L, t) = 0$$

$$v(x=x_b, t) = y_b \qquad \text{for } t \geqslant 0$$

we consider the complex transformation which maps the complex upper half-plane (described by the complex variable $z = X + iY$) to the region in figure 6(*a*). It is the following Schwartz–Christoffel transformation

$$\omega = i[(1-\rho)\ln(1-\rho)/\rho + \ln 2\rho - \rho \ln(z-1) - (1-\rho)\ln(z+1)] \qquad \text{(A1.1)}$$

where $\rho = x_b/L$ and we have taken $L = \pi$ for convenience. Equation (A1.1) maps the real axis ($Y = 0$) onto the boundary of the region in figure 6(*a*). Figures 6(*a*) and 6(*b*) illustrate the detailed form of this transformation.

The solution of our Dirichlet problem is then given by the imaginary part of the complex function

$$F = \frac{y_b}{\pi}[\ln(z-1) - \ln(z+1)]. \qquad \text{(A1.2)}$$

Let us first concentrate on the case $\rho = \frac{1}{2}(x_b = \frac{1}{2}L)$. The transformation (A1.1) takes the simple form

$$\omega_0 = -\tfrac{1}{2}i[\ln(z-1) + \ln(z+1)]. \qquad \text{(A1.3)}$$

We shall be using the complex variable $\omega_0 = x_0 + it_0$ for the case $\rho = \frac{1}{2}$ and reserve the notation $\omega = x + it$ for the general case, where ρ can take arbitrary values.

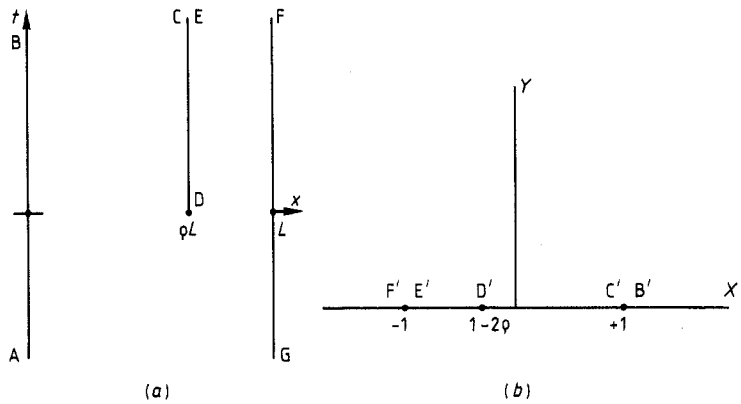

Figure 6. The $\omega=(x, t)$ and $z=(X, Y)$ complex planes as used throughout appendix 1.

According to equations (24), (25) we have

$$f_c(\rho=\tfrac{1}{2})v_b^2=2\lim_{\substack{T\to+\infty\\T_1\to+\infty}}\left\{\tfrac{1}{2}\int_{x_0=0}^{\pi}\int_{t_0=-T}^{T_1}\left[\left(\frac{\partial v}{\partial x_0}\right)^2+\left(\frac{\partial v}{\partial t_0}\right)^2\right]dt_0\,dx_0\right.$$

$$\left.-\tfrac{1}{2}\int_{x_0=0}^{\pi}\int_{t_0=0}^{T_1}\frac{4v_b^2}{\pi^2}\,dt_0\,dx_0\right\}. \tag{A1.4}$$

In the last expression the first term comes from the area of the surface described by the equation $v=v(x_0, t_0)$, where the area is calculated by means of the harmonic approximation (equation (11)). The second term comes from the areas of the rectangles covered by the two final state strings, if these strings are allowed to propagate freely for a very long time. Note that these areas too are to be calculated by the same method of approximation.

The quantity

$$\int_{R_0}\int\left[\left(\frac{\partial v}{\partial x_0}\right)^2+\left(\frac{\partial v}{\partial t_0}\right)^2\right]dt_0\,dx_0$$

where R_0 is an arbitrary region in the ω_0 plane, is equal to

$$\int\int_{\xi}d\mathrm{Re}F\,d\mathrm{Im}F$$

where ξ is the image of R_0 in the $(\mathrm{Re}F, \mathrm{Im}F)$ complex plane. It thus represents the area of the flat surface ξ. In order to evaluate the limit appearing in equation (A1.4) we need to know the asymptotic behaviour of F for $t_0=T_1\to\infty$ and $t_0=T\to\infty$. Using equations (A1.2) and (A1.3) we readily find

$$\mathrm{Re}F\to\begin{cases}v_b\left(\dfrac{2T_1}{\pi}+\dfrac{2\ln 2}{\pi}\right) & \text{for } 0<x_0<\pi/2 \quad T_1\to\infty\\[2ex] v_b\left(-\dfrac{2T_1}{\pi}-\dfrac{2\ln 2}{\pi}\right) & \text{for } \pi/2<x_0<\pi \quad T_1\to\infty\end{cases} \tag{A1.5}$$

with $\mathrm{Im}F$ varying linearly with x_0 as $T_1\to\infty$. We also find that $F\to 0$ for $T\to\infty$.

We conclude that the part of the ω_0 plane which is bounded by the lines $x_0=0$, $x_0=\pi$, $x_0=\pi/2$ (for $t_0>0$), $t_0=T_1$ and $t_0=T$ maps asymptotically (for $T\to\infty$ and $T_1\to\infty$) onto a rectangle in the (ReF, ImF) complex plane. The area of this rectangle is $y_b^2[(4T_1/\pi)+(4\ln 2/\pi)]$, so

$$\int_{x_0=0}^{\pi}\int_{t_0=-T}^{T_1}\left[\left(\frac{\partial v}{\partial x_0}\right)^2+\left(\frac{\partial v}{\partial t_0}\right)^2\right]\mathrm{d}t_0\,\mathrm{d}x_0\to y_b^2\left(\frac{4T_1}{\pi}+\frac{4\ln 2}{\pi}\right). \tag{A1.6}$$

Equation (A1.4) now yields

$$f_c(\rho=\tfrac{1}{2})=4\ln 2/\pi. \tag{A1.7}$$

We can use this partial result to calculate f_c for arbitrary values of ρ.

Using the transformations (A1.1) and (A1.3) we can establish a mapping of the physically interesting region $(0<x<\pi)$ of the (x, t) plane (for arbitrary ρ) onto the region $0<x_0<\pi$ of the (x_0, t_0) plane ($\rho=\frac{1}{2}$). We can also use these transformations to find the asymptotic behavour of the variable $\omega=(x, t)$ corresponding to the segments defined by the equation $t_0=T_1(\to+\infty)$. We readily find

$$\omega=\mathrm{i}C(\rho)+\omega_0+\mathrm{i}\pi gF/y_b \tag{A1.8}$$

where we have put $g=-\rho+\frac{1}{2}$ and

$$C(\rho)=(1-\rho)\ln\left(\frac{1-\rho}{\rho}\right)+\ln 2\rho. \tag{A1.9}$$

Equations (A1.5) and (A1.9) now yield

$$t\to\begin{cases}2(1-\rho)t_0+2g\ln 2+C(\rho) & 0<x<\rho\pi\\ 2\rho t_0-2g\ln 2+C(\rho) & \rho\pi<x<\pi\end{cases} \tag{A1.10}$$

for $t_0=T_1\to+\infty$. It follows that for large t_0 the mapping $\omega_0\to\omega$ causes independent parallel shifts of the two segments (to the left and to the right of the breaking axis) of the line of constant x_0. Using this fact we can now write the difference

$$y_b^2 f_c(\rho)-y_b^2 f_c(\rho=0)$$

as follows

$$\begin{aligned}\lim_{T_1\to\infty}\Bigg(y_b^2\Bigg\{&\int_{x=0}^{\pi}\int_{t=-\infty}^{t(T_1,x_0)}\left[\left(\frac{\partial v}{\partial x}\right)^2+\left(\frac{\partial v}{\partial t}\right)^2\right]\mathrm{d}t\,\mathrm{d}x\\ &-\int_{x=0}^{\rho\pi}\int_{t=0}^{t(T_1,x_0)}\left(\frac{1}{\rho^2\pi^2}\right)\mathrm{d}t\,\mathrm{d}x-\int_{x=\rho\pi}^{\pi}\int_{t=0}^{t(T_1,x_0)}\left(\frac{1}{(1-\rho)^2\pi^2}\right)\mathrm{d}t\,\mathrm{d}x\Bigg\}\\ &-y_b^2\left\{\int_{x_0=0}^{\pi}\int_{t_0=-\infty}^{T_1}\left[\left(\frac{\partial v}{\partial x_0}\right)^2+\left(\frac{\partial v}{\partial t_0}\right)^2\right]\mathrm{d}t_0\,\mathrm{d}x_0\right.\\ &\left.-\int_{x_0=0}^{\pi}\int_{t_0=0}^{T_1}\left(\frac{4}{\pi^2}\right)\mathrm{d}t_0\,\mathrm{d}x_0\right\}\Bigg)\end{aligned} \tag{A1.11}$$

where the t integration in the first three integrals extends up to the image under the transformation $\omega_0\to\omega$ of the segments defined by $t_0=T_1$.

Notice that the two integrals containing derivatives of the function v are equal, since they can both be written in the form $\iint_{R_0}\mathrm{d}\mathrm{Re}F\,\mathrm{d}\mathrm{Im}F$, where R_0 is a certain region in the

$(\mathrm{Re}F, \mathrm{Im}F)$ plane. On performing the remaining trivial integrations and using equation (A1.10) we obtain the advertised result

$$f_c(\rho)=(1/\pi)\ln\left[(1-\rho)^{-1/\rho}\rho^{-1/(1-\rho)}\right]. \tag{A1.12}$$

Appendix 2

In this appendix we calculate the continuum limit κ_c of the quantity $\kappa(N, N_b)$.

In the region M depicted in figure 7(*a*), we introduce the complex variable $\omega=x+it$. It will be useful to consider a complex (Schwartz–Christoffel) transformation which maps the complex upper half-plane ($z=X+iY$, $Y\geqslant 0$) onto the region M, namely

$$\omega=A\int\frac{z-p}{(z-a)^{1/2}(z+a)^{1/2}}\,\frac{1}{z^2-1}\,dz+B. \tag{A2.1}$$

The exact way in which the real axis $Y=0$ is mapped onto the boundary of the region M is illustrated in figure 7.

The parameters A, p, a, can be easily determined from the geometrical figures of M. We may integrate equation (A2.1) to obtain

$$\mathrm{Im}\,\omega=t=\frac{A}{(a^2-1)^{1/2}}\left((1-p)\ln\left|\frac{2(a^2-1)^{1/2}(a^2-z^2)^{1/2}-2z+2a^2}{z-1}\right|\right.$$
$$\left.+(1+p)\ln\left|\frac{2(a^2-1)^{1/2}(a^2-z^2)^{1/2}+2z+2a^2}{z+1}\right|\right)+B$$

for z real and $-a<z<a$.

Considering the jumps in the imaginary parts of the logarithms at $z=+1$ and $z=-1$, we can determine A and p. We find

$$A=(L/\pi)(a^2-1)^{1/2}\qquad p=1-2\rho.$$

a is determined by considering the difference $t(z=1-2\rho)-t(z=a)$. Since the point $z=1-2\rho$ corresponds to the endpoint of the breaking axis, this difference is equal to T.

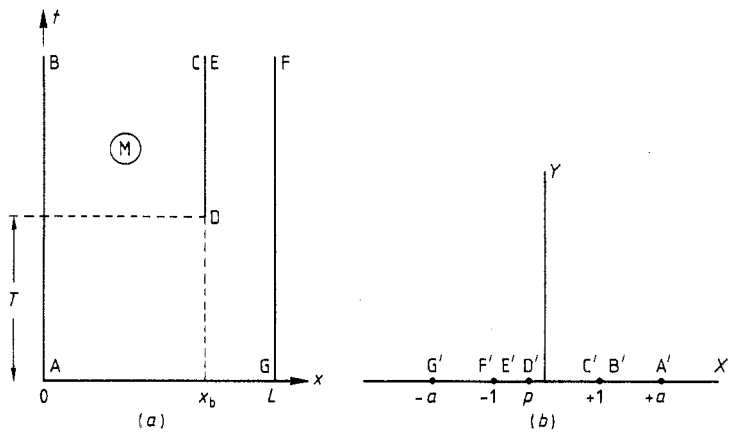

Figure 7. The $\omega=(x, t)$ and $z=(X, Y)$ complex planes as used throughout appendix 2.

We can thus determine a as a function of T. It is obvious that a grows with T. Since we are directly interested in results valid for large values of T, we calculate $1/a$ to first order in $\exp(-\pi T/L)$. We find

$$1/a = \frac{\exp(-\pi T/L)}{\rho^{\rho}(1-\rho)^{1-\rho}}. \tag{A2.2}$$

In order to calculate κ_c we need, according to the discussion in § 3, to introduce a harmonic function $V(x, t)$ which obeys the boundary conditions

$$V(0, t) = V(L, t) = 0 \tag{A2.3}$$

$$V(\rho L, t) = y_b \qquad \text{for } t > T \tag{A2.4}$$

$$V(x, 0) = -h \sin(\pi x/L). \tag{A2.5}$$

This Dirichlet problem can be solved in principle by using the transformation (A2.1) and then working with a Dirichlet problem in the upper half-plane. The boundary condition (A2.5), however, looks quite complicated in terms of the variable z. It is therefore more convenient to introduce a harmonic function which has a simple form in terms of z and, while obeying equations (A2.3) and (A2.4), satisfies equation (A2.5) only in the limit $T \to \infty$, which is the appropriate limit we need in order to calculate κ_c. This is done as follows. Consider as a first step the analytic complex function $H(r) = H(x_0 + it_0)$ defined on the semi-infinite strip $t_0 \geqslant 0$, $0 < x_0 < L$, the real part of which is bounded everywhere and satisfies the boundary conditions

$$\begin{aligned} &\operatorname{Re} H(it_0) = \operatorname{Re} H(L + it_0) = 0 \\ &\operatorname{Re} H(x_0) = -h \sin(\pi x_0/L). \end{aligned} \tag{A2.6}$$

This function is given by the formula

$$H(r) = -ih \exp\left(\frac{i\pi r}{L}\right). \tag{A2.7}$$

Using the transformation which maps the semi-infinite strip onto the complex upper half-plane, namely

$$r = -\frac{aL}{\pi} \int \frac{1}{z} \frac{1}{(z-a)^{1/2}} \frac{1}{(z+a)^{1/2}} \, dz \tag{A2.8}$$

(where the corners of the strip correspond to the points $z = a$ and $z = -a$ of the upper half-plane) and putting $H(r) = G(z)$. We can then consider the function

$$J(z) = G(z) - \frac{iy_b}{\pi} [\ln(z-1) - \ln(z+1)]. \tag{A2.9}$$

Regarding $J(z)$ as a function of $\omega = x + it$ (via the transformation (A2.1)) we note that the real part of $J(z)$ is harmonic and it obeys the boundary conditions (A2.4) and (A2.5). Furthermore it is bounded everywhere in the region M and because of the way in which it was constructed, it satisfies equation (A2.5) asymptotically for $T \to +\infty$.

It is useful to have in mind the exact form of $\operatorname{Re} J$ and $\operatorname{Im} J$ as functions of z for real z (corresponding to points on the boundary of the region M in figure 7(*a*)). Using equations (A2.7), (A2.8) and (A2.9) we find:

For z real and $z \notin [-a, a]$

$$\begin{aligned} \mathrm{Re}J &= -h(1-a^2/z^2)^{1/2} \\ \mathrm{Im}J &= ha/z - y_b/\pi[\ln(z-1) - \ln(z+1)]. \end{aligned} \tag{A2.10}$$

For z real, $-a < z < a$

$$\begin{aligned} \mathrm{Im}J &= h\frac{z}{a+(a^2-z^2)^{1/2}} - \frac{y_b}{\pi}[\ln(z-1) - \ln(z+1)] \\ \mathrm{Re}J &= \begin{cases} 0 \text{ for } z \notin [-1, 1] \\ y_b \text{ for } -1 < z < 1. \end{cases} \end{aligned} \tag{A2.11}$$

We now calculate the area of the part of our surface which is enclosed by the boundary of the region M in figure 7(*a*) and two segments of constant and large $t-T$. For $x=0$ and $x=L$ large $t-T$ corresponds to z real and $z=1+\varepsilon_1$, $z=-1-\varepsilon_2$ with ε_1 and ε_2 small. ε_1 and ε_2 can be expressed as functions of t by means of equation (A2.2). Lines of constant $t-T$ in the ω plane map onto asymptotically straight segments of constant $\mathrm{Im}J$ in the ($\mathrm{Re}J$, $\mathrm{Im}J$) plane. In this plane our surface maps onto the region shown in figure 8. This consists of a rectangle and a shape which tends to a semicircle of radius h for $a \to \infty$. The area A_e (equation (30)) of our surface

$$A_e = Lt + \tfrac{1}{2}\int\int \mathrm{d}\mathrm{Re}J\, \mathrm{d}\mathrm{Im}J$$

can be calculated by taking into account the equations which give $\mathrm{Re}J$ and $\mathrm{Im}J$ as a function of J on the boundary of figure 8. For our purpose we need only retain terms of first order in $1/a \propto \exp(-\pi T/L)$. We find that

$$A_e = Lt - \frac{y_b^2}{2\pi}(\ln\varepsilon_1 + \ln\varepsilon_2) + \frac{y_b^2}{\pi}\ln 2 + \frac{h^2\pi}{4} + \frac{hy_b}{a} + \ldots \tag{A2.12}$$

The first three terms in the RHS of the last equation correspond to the area A_0 of equation (30). Hence we have

$$\exp[-b(A_e - A_0)] = \exp(-bh^2\pi/4)\left(1 - \frac{hy_b b}{\rho^\rho(1-\rho)^{1-\rho}}\exp(-\pi T/L)\right). \tag{A2.13}$$

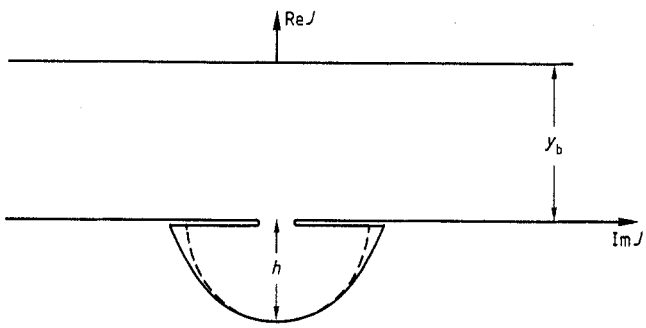

Figure 8. The image of the surface $y_1 = \mathrm{Re}J$ in the ($\mathrm{Re}J$, $\mathrm{Im}J$) complex plane (see appendix 2).

Comparing with equation (30) we find

$$(\pi b)^{1/2}\,\frac{\gamma^1_{00}}{\gamma^0_{00}}=\frac{y_b b}{\rho^\rho(1-\rho)^{1-\rho}}$$

that is

$$\frac{\gamma^1_{00}}{\gamma^0_{00}}=\frac{y_b\sqrt{b}}{\sqrt{\pi}}\,\frac{1}{\rho^\rho(1-\rho)^{1-\rho}}. \tag{A2.14}$$

Comparing with equation (7) of § 2 and taking into account that κ in equation (7) is the coefficient of $y_b^{\pm}=y_{1,b}\pm y_{2,b}$, we find the result

$$\kappa_c=[(2\pi)^{1/2}\rho^\rho(1-\rho)^{1-\rho}]^{-1}.$$

References

[1] Isgur N and Paton J 1985 *Phys. Rev.* D **31** 2910 and references cited therein
[2] Kogut J and Susskind L 1975 *Phys. Rev.* D **11** 395
[3] Micu L 1961 *Nucl. Phys.* B **10** 521
Le Youanc A, Oliver L, Pene O and Raynal J C 1973 *Phys. Rev.* D **8** 2223; 1974 *Phys. Rev.* D **9** 1415
[4] Isgur N and Kokoski R 1985 *University of Toronto Report*
[5] Isgur N, Kokoski R and Paton J 1985 *Phys. Rev. Lett.* **54** 869
[6] Perantonis S 1986 unpublished
[7] Luscher M and Symanzik K 1980 *Nucl. Phys.* B **173** 365
[8] Mandelstam S 1973 *Nucl. Phys.* B **64** 205
[9] Merlin J 1986 *DPhil Thesis* University of Oxford
[10] Hasenfratz P, Horgan R R, Kuti J and Richard J M 1980 *Phys. Lett.* **95B** 299
[11] Shifman M, Vainshtein A and Zakharov V 1979 *Nucl. Phys.* B **147** 385, 447, 519